Scale-up and Modeling of Fixed-Bed Reactors for Catalytic Phenol Oxidation over Adsorptive Active Carbon

Somsaluay Suwanprasop,[†] Athanasios Eftaxias,[‡] Frank Stüber,*[,‡] Isabelle Polaert,[†] Carine Julcour-Lebigue,[†] and Henri Delmas[†]

Laboratoire de Génie Chimique, UMR CNRS 5503, 5 rue Paulin Talabot, 31106 Toulouse, France, and Departament d'Enginyeria Química, ETSEQ, Universitat Rovira i Virgili, Av. dels Països Catalans 26, 43007 Tarragona, Catalunya, Spain

The wet air oxidation of phenol over a commercial active carbon catalyst has been studied in laboratory-scale and pilot-plant fixed-bed reactors at mild temperatures and oxygen partial pressures of 120−160 °C and 0.05−0.2 MPa, respectively. The performances of the fixed-bed reactors have been assessed and compared to each other for both up- and downflow operation mode. Depending on the flow mode and reactor scale, distinct phenol destruction rates have been observed in the experiments. A series of batch experiments are carried out to obtain phenol removal kinetics, which are subsequently implemented in the modeling of the pilot-plant fixed-bed reactor. A one-dimensional, nonisothermal piston dispersion model is developed to describe in detail the interplay of reaction kinetics, gas−liquid hydrodynamics, and heat and mass transfer in both flow directions. The model predicts reasonably well the experimental data, thus allowing for a thorough explanation of the observed pilot-plant reactor performance.

1. Introduction

The increasing release of organic pollutants contained in many industrial end stream effluents has been the driving force for developing alternative effluent treatments prior to their discharge to conventional biofilters or sewage plants. A suitable destruction of such pollutants is catalytic wet air oxidation (CWAO) at mild operating conditions and attractive process economics.[1] Recently, catalysts with improved stability in CWAO of phenol and various substituted phenols have been developed based on noble metals,[2] mixed oxides,[3] or active carbon (AC).[4] By employment of AC, unit operations of adsorption and reaction are naturally combined in an adsorptive oxidation reactor. CWAO over AC becomes especially attractive when integrated in adsorption−oxidation cycles[5] or biological end treatments[6] because complete mineralization of organic pollutants by CWAO alone is no longer required.

In most CWAO studies,[4,7−9] fixed-bed reactors (FBRs) have been preferred over slurry or fluidized-bed reactors. Also, several aromatic pollutants show the ability to undergo homogeneous condensation reactions via oxidative coupling,[10] and large catalyst-to-liquid ratios as in FBRs are required to limit these side reactions and fast catalyst deactivation.[9] To properly design and operate industrial CWAO units, the pilot-plant reactor performance and modeling of continuous FBRs must be assessed. At present, most of the work on CWAO has been focused on catalysts and kinetic analysis rather than on the understanding of the overall reactor performance.[11] The studies that are related to process analysis often cover only a specific reactor aspect,[8,9] simplify reactor modeling,[12] or do not provide any experimental results to support model predictions.[13]

Thus, the aim of this work is to thoroughly investigate CWAO of phenol over AC in both a small-scale and a pilot-plant FBR and to carry out detailed reactor modeling to understand the complex interplay of reaction kinetics, intraparticle and interphase heat and mass transfer, and gas−liquid hydrodynamics.

2. Experimental Section

2.1. Materials. Deionized water and analytical-grade phenol (Aldrich) are used to prepare 5 g/L phenol solutions. The oxidant was either compressed high-purity air (Carburos Metalicos, Linde Gas) or pure oxygen mixed with pure nitrogen (Linde Gas). AC (d_p = 1.5 or 2.5 mm) was purchased from Merck (Reference Nos. 2514 and 2518; ash content 3.75%; Brunauer−Emmett−Teller specific surface area 990 m^2/g; pore volume 0.55 cm^3/g; mean pore diameter 1.4 nm). Phenol adsorption tests under an air atmosphere have shown a maximum capacity of 370 mg_{Ph}/g_{AC} at 20 °C. Prior to experiments in a small-scale trickle-bed reactor (TBR), the AC particles are crushed and sieved to obtain the 0.3−0.7 mm fraction. Each sample is washed, dried at 110 °C for 12 h, and stored under an inert atmosphere at room temperature. For the pilot-plant experiments and batch kinetic study, the 1.5 mm particles are sieved to get the 1.25−1.6 mm fraction (D[4,3] = 1.0 mm by Mastersizer 2000, Malvern).

2.2. Catalytic Reactors and Operating Conditions Used. Table 1 gives the range of operating conditions used in the kinetic and scale-up studies.

Batch Basket Reactor. For the determination of intrinsic kinetic parameters, batch phenol oxidation is performed in a stirred autoclave (Parr Instruments) using the 1.25−1.6 mm fraction of AC to reduce fast and continuous catalyst deactivation as previously reported with powder.[9] Details on experiments (see also Table 1) and results are presented elsewhere.[14]

* To whom correspondence should be addressed. Tel.: 34 977 559671. Fax: 34 977 559677. E-mail: fstuber@etseq.urv.es.
[†] UMR CNRS 5503.
[‡] Universitat Rovira i Virgili.

Table 1. Reactor Type and Operating Conditions Used in the Kinetic and Scale-up Study

	batch reactor	small reactor	pilot plant
V, cm^3	300	20	600
D_R, cm	6.2	1.1	2.54
L_R, cm	10	20	120
W_{cat}, kg	9×10^{-3}	7×10^{-3}	0.325
d_p, mm	$D[4,3] = 1.0$	0.5	$D[4,3] = 1.0$
ϵ_p	0.53	0.53	0.53
$C_{Ph,0}$, g/L	2.5−5	5	5
P_{O_2}, MPa	0.1−0.35	0.1−0.2	0.05−0.2
T, °C	130−160	120−160	120−160
Q_G, NL/h	60	9	50−200
u_g, mm/s		5	5−25
F_L, kg/h		0.015−0.15	0.5−3.5
u_l, mm/s		0.04−0.5	0.3−2
τ, h		0.04−0.6	0.1−0.7
G−L flow		up, down	up, down

Laboratory-Scale FBR. CWAO of 5 g/L phenol solutions has first been conducted in a small laboratory-scale reactor placed in a temperature-controlled oven (±1 °C). The reactor is filled with 6.6−7 g of AC retained between two sintered metal disks. A detailed reactor scheme is available elsewhere.[15] The oxidation tests have been performed in downflow and upflow modes at constant temperature (120, 140, and 160 °C) and oxygen partial pressure (0.1 and 0.2 MPa). The air flow rate is set at 2.4 mL/s (STP) to ensure 100−250% oxygen excess for complete phenol oxidation. The liquid flow rates selected correspond to space times and liquid superficial velocities of 0.04−0.6 h and 0.04−0.55 mm/s, respectively. At a fixed liquid flow rate, the reactor is rapidly heated, while saturation of the AC bed with phenol and oxidation reactions requires 20 h to reach steady state. To obtain conversion−space time profiles, the liquid flow rate is varied. After each change, the evolution of the phenol concentration is monitored to detect the new steady state of the reaction, which, depending on the liquid flow rate, is achieved within 2−4 h. The liquid-phase composition is immediately analyzed by taking three samples at steady-state conditions. The experimental error in the phenol and chemical oxygen demand (COD) concentrations is evaluated to be ±5%.

Pilot-Plant Reactor. A pilot-plant reactor of 2.5 cm diameter and 120 cm length (see Figure 1) has been designed, constructed, and tested. The reactor tube is filled with 325 g of AC. The reactor tube is covered with a double-jacket annular heater, where hot thermal oil at 120−160 °C oil is pumped through at a high flow rate. Nonisothermal reactor operation results from feeding of the gas−liquid mixture at room temperature. The oxygen partial pressure ranges from 0.05 to 0.2 MPa, the liquid space time from 0.1 to 0.7 h corresponding to superficial velocities of 0.3−2 mm/s, and the inlet gas superficial velocity from 5 to 25 mm/s. The pilot unit is designed to operate in upflow and downflow modes of gas−liquid flow by means of five three-way valves located along the gas and liquid circuits (see Figure 1).

Several temperature sensors and sampling valves have been mounted along the reactor to measure the concentration and temperature axial profiles under nonisothermal conditions and wall-to-bed heat transfer in both flow modes. Liquid sampling is also done after the gas−liquid separator. To vary the oxygen partial pressure, the total pressure (measured in the gas outlet of the separator and controlled by a proportional−integral−derivative) and/or the composition of the O_2/N_2 inlet mixture are adequately adjusted. Gas and liquid flow rates are set and measured by mass flow controllers and a precision liquid pump and balance, respectively.

The start-up of oxidation experiments in the pilot plant consists of saturating first the AC for 10 h under a nitrogen atmosphere at reaction temperature. Once

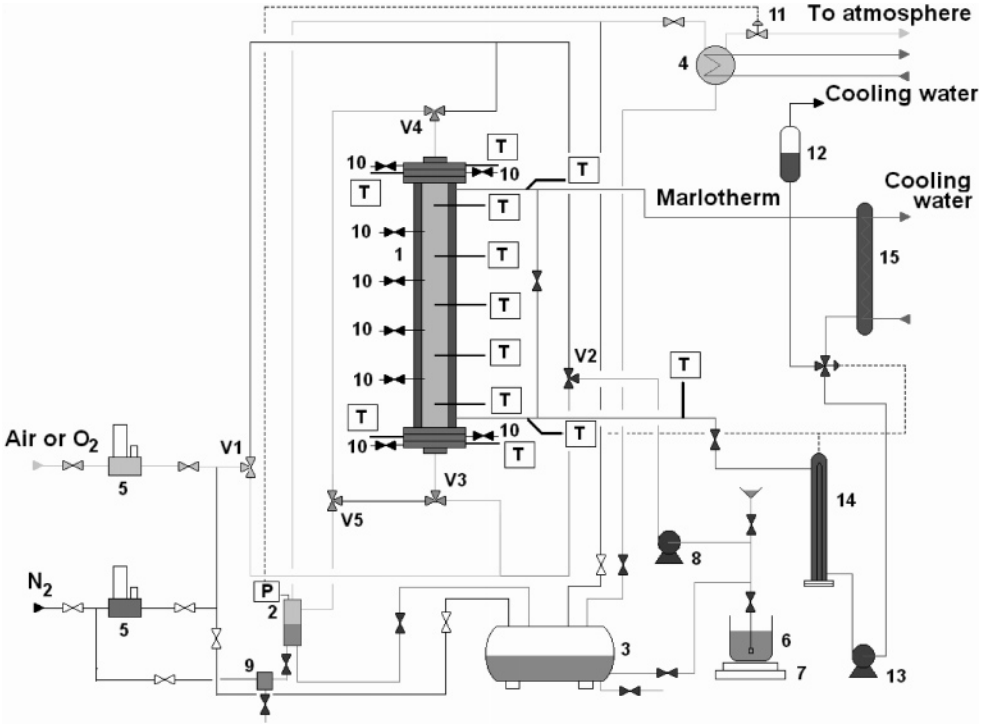

Figure 1. Experimental pilot-plant reactor (upflow mode): (1) jacketed packed-bed column; (2) gas−liquid separator; (3) liquid storage tank; (4) condenser; (5) gas mass flow controllers; (6) feed tank; (7) balance; (8) dosing pump; (9) sampling device; (10) liquid sample valves; (11) pneumatic valve; (12) expansion vase; (13) gear pump; (14) heater; (15) cooling exchanger; (V1−V5) three-way valves for upflow or downflow mode.

the phenol breakthrough is observed, air or a O_2/N_2 mixture is fed instead of nitrogen. The phenol concentration at the reactor outlet is measured each 30 min until steady state of the reaction is reached (after 1−4 h depending on the operating conditions). Then, the liquid or gas flow rate is set to a new value. In this way, about 50 experiments have been carried out to investigate the influence of temperature, oxygen pressure, gas and liquid flow rates, and flow direction on the reactor performance. During the experiments, liquid and gas flow rates and temperatures are monitored online using a microcomputer data acquisition system.

2.3. Analysis. Exit liquid samples are analyzed with a high-performance liquid chromatograph using a C_{18} reverse-phase column (Spherisob ODS-2 or ProntoSIL C18 AQ) to obtain concentrations of phenol and intermediates. The separation is achieved with a mobile phase of variable composition programmed at 1 mL/min, using as eluants acidified deionized water and acetonitrile or methanol. Compounds are detected with UV at wavelengths of 210 nm (intermediates) and 254 nm (phenol). A standard mixture of phenol and oxidation products is periodically tested. The liquid stream is also analyzed for the remaining COD.

3. Model Development

3.1. Kinetic Model. In agreement with previous kinetic studies,[15] a simple power law is convenient to accurately describe the phenol destruction over AC assuming a first order of phenol, while the oxygen order has to be determined by the optimization algorithm. The first order of phenol is also confirmed when plotting the logarithm of the phenol concentration as a function of time (not shown here). The following rate equation can thus be proposed:

$$R_{\text{phenol}} = -k_0 \exp\left(\frac{-E}{RT}\right) C_{\text{Ph}} x_{\text{O}_2}^{\alpha} \tag{1}$$

The values of the Weisz modulus ($0.45 < \phi' < 1.5$) at the initial time, with oxygen being the limiting reactant, indicate that the reaction occurs in the intermediate diffusion regime. The intrinsic kinetics of phenol oxidation is thus derived using a batch reactor model that accounts for transient diffusion of both oxygen and phenol inside the catalyst pores.[16] In the model, spherical geometry is assumed with $D[4,3] = 1.0$ mm as the reference diameter and a tortuosity value of 3 to evaluate the effective diffusivities of oxygen and phenol.

A 0.5 oxygen order has been identified to match best the phenol concentrations obtained at 140 °C and 0.1−0.35 MPa of oxygen partial pressure. The activation energy and frequency factor for phenol oxidation are respectively 74 kJ/mol and 3.75×10^5 m^3/(s kg).

3.2. Reactor Model. The present nonisothermal model is based on previous work.[13,15] The model parameters of interest are the axial liquid-phase temperature and the axial liquid-phase concentrations of dissolved oxygen and organic compounds, in particular the conversion of the phenol reactant. The model reflects the complex interplay of reaction kinetics, gas−liquid hydrodynamics, and heat and mass transfer on both the pellet and reactor length scales. Splitting of the total liquid holdup into stagnant and dynamic parts, as well as partial wetting for the downflow mode, is considered to establish weighted effectiveness factors that address both the gas- and liquid-limiting reactant situation. Furthermore, to simulate nonisothermal reactor operation, two limiting cases of water vaporization are described, i.e., instantaneous vapor−liquid equilibrium and progressive axial saturation of the gas phase with water.

On the whole, the model accounts for (i) static and dynamic liquid portions, (ii) constant partial catalyst wetting in a trickle-flow regime throughout the reactor; (iii) axial dispersion in the dynamic liquid phase; (iv) pore diffusion and gas−liquid and liquid−solid mass transfer; (v) axial concentration and temperature gradients but no radial gradients ($D_R/d_p = 25$); (vi) heat transfer between the catalytic fixed bed and reactor wall (at constant wall temperature); (vii) instantaneous water vapor−liquid equilibrium or mass-transfer-limited axial saturation of the gas phase with water.

The following assumptions have been made in the model development: (i) stable catalyst activity; (ii) complete internally wetted catalyst pores; (iii) no temperature gradient between the gas, liquid, and catalyst; (iv) negligible pressure drop, i.e., the total pressure is constant; (v) ideal gas-phase behavior; (vi) nonvolatile organic reactants.

For simulations presented in the following sections, only complete mineralization of the reacted phenol to H_2O and CO_2 is considered because intermediates represent in most cases less than 20% of total COD and do not significantly increase at high phenol conversion.

Pellet-Scale Model. For simultaneous diffusion and reaction of reactants and products within the liquid-filled pores, the following mass balance equation has been solved, assuming spherical symmetry:

$$\frac{1}{r^2}\frac{\mathrm{d}}{\mathrm{d}r}\left(r^2 D_j^{\text{eff}} \frac{\mathrm{d}C_j}{\mathrm{d}r}\right) + \rho_{\text{p}} R_j = 0 \tag{2}$$

with boundary conditions at $r = 0$

$$\left.\frac{\mathrm{d}C_j}{\mathrm{d}r}\right|_{r=0} = 0 \tag{3}$$

and $r = r_{\text{p}}$

$$C_j|_{r=r_{\text{p}}} = C_j^*$$

$$D_j^{\text{eff}} \left.\frac{\mathrm{d}C_j}{\mathrm{d}r}\right|_{r=r_{\text{p}}} = k_{j\text{ls}}^{\text{d}} f_{\text{d}} (C_j^{\text{d}} - C_j^*) + k_{j\text{ls}}^{\text{s}} f_{\text{s}} (C_j^{\text{s}} - C_j^*) + [k_{\text{gs}}(1-f)(C_{\text{O}_2}^{\text{g}} - HC_{\text{O}_2}^*)]_{\text{only for O}_2} \tag{4}$$

Equation 4 accounts thus for the effect of stagnant liquid pockets and partial wetting without the need of assuming a limiting reactant. However, this approach considers a uniform concentration of reactants on the catalyst surface (required by the use of a one-dimensional diffusion model) assuming infinite tangential diffusion. Equation 4 for the boundary condition at the particle surface is based on the reactant concentration j in the liquid or gas bulk, which has to be calculated by the reactor-scale model. To link the fluid and surface concentrations of each compound j, a weighted effectiveness factor that accounts for the fluid−solid mass-transfer resistance is defined for each of the fractions of the pellet surface in contact with the liquid or gas phase:

$$\eta_j^{\mathrm{d}} = \frac{3k_{j\mathrm{ls}}^{\mathrm{d}} f_{\mathrm{d}}(C_j^* - C_j^{\mathrm{d}})}{r_{\mathrm{p}}\rho_{\mathrm{p}} R_j^*}$$

$$\eta_j^{\mathrm{s}} = \frac{3k_{j\mathrm{ls}}^{\mathrm{s}} f_{\mathrm{s}}(C_j^* - C_j^{\mathrm{s}})}{r_{\mathrm{p}}\rho_{\mathrm{p}} R_j^*}$$

$$\eta_{\mathrm{O_2}}^{\mathrm{g}} = \frac{3k_{\mathrm{gs}}(1-f)(HC_{\mathrm{O_2}}^* - C_{\mathrm{O_2}}^{\mathrm{g}})}{r_{\mathrm{p}}\rho_{\mathrm{p}} R_{\mathrm{O_2}}^*} \tag{5}$$

Reactor-Scale Model. Axial dispersion in the liquid phase can alter the reactor performance, and the one-dimensional piston dispersion exchange (PDE) model has been used. The gas phase is assumed to be in plug flow. If catalyst wetting is not complete as in the trickle-bed regime, the following equation results for the oxygen gas-phase concentration:

$$\frac{\mathrm{d}(u_{\mathrm{g}} C_{\mathrm{O_2}}^{\mathrm{g}})}{\mathrm{d}z} + (k_{\mathrm{L}}a)\left(\frac{C_{\mathrm{O_2}}^{\mathrm{g}}}{H} - C_{\mathrm{O_2}}^{\mathrm{d}}\right) - \eta_{\mathrm{O_2}}^{\mathrm{g}}\rho_{\mathrm{b}} R_{\mathrm{O_2}}^* = 0 \tag{6}$$

The dynamic liquid concentrations are given by the following mass balance equation, which includes axial dispersion:

$$-D^{\mathrm{ad}}\epsilon_{\mathrm{ld}}\frac{\mathrm{d}^2 C_j^{\mathrm{d}}}{\mathrm{d}z^2} + \frac{\mathrm{d}(u_{\mathrm{l}} C_j^{\mathrm{d}})}{\mathrm{d}z} + (ka)_{j\mathrm{ll}}(C_j^{\mathrm{d}} - C_j^{\mathrm{s}}) - \eta_j^{\mathrm{d}}\rho_{\mathrm{b}} R_j^* - \left[k_{\mathrm{L}}a\left(\frac{C_{\mathrm{O_2}}^{\mathrm{g}}}{H} - C_{\mathrm{O_2}}^{\mathrm{d}}\right)\right]_{\text{only for } \mathrm{O_2}} = 0 \tag{7}$$

For the stagnant liquid pockets that may exist on the reactor length scale, the convection term drops out and algebraic equations describe the stagnant liquid concentrations:

$$(ka)_{j\mathrm{ll}}(C_j^{\mathrm{d}} - C_j^{\mathrm{s}}) + \eta_j^{\mathrm{s}}\rho_{\mathrm{b}} R_j^* = 0 \tag{8}$$

Finally, on the basis of work by Van Gelder et al.,[17] the energy balance for the pseudohomogeneous gas–liquid fluid incorporating water evaporation and bed-to-wall heat transfer gives

$$(u_{\mathrm{l}}\rho_{\mathrm{l}}c_{\mathrm{pl}} + u_{\mathrm{g}}\rho_{\mathrm{g}}c_{\mathrm{pg}})\frac{\mathrm{d}T}{\mathrm{d}z} + \frac{\varphi}{A}\Delta H^{\mathrm{v}} - \rho_{\mathrm{b}}\sum r_i^{\mathrm{ap}}(-\Delta H_i) + \frac{h_{\mathrm{w}}A}{V_{\mathrm{R}}}(T - T_{\mathrm{w}}) = 0 \tag{9}$$

The apparent rate of the ith reaction (r_i^{ap}) is calculated from stoichiometry and the compound overall reaction rates ($\eta_j R_j$). Here, as mentioned before, only one reaction of complete oxidation is considered. With the thermal fluid being circulated at a high flow rate through the thermally isolated double jacket, the reactor wall temperature remains constant.

The water evaporation rate (φ) per unit reactor length is determined assuming that the gas stream either reaches instantaneously liquid–vapor equilibrium or is progressively saturated while flowing through the catalytic fixed bed.

When the total molar gas flow rate is denoted by $\dot{n}_{\mathrm{T}}^{\mathrm{g}}$ and the water vapor molar flow rate by $\dot{n}_{\mathrm{H_2O}}^{\mathrm{g}}$, then the following equality must always be fulfilled in the case of instantaneous saturation of the gas stream with water vapor:

$$\frac{\dot{n}_{\mathrm{H_2O}}^{\mathrm{g}}}{\dot{n}_{\mathrm{T}}^{\mathrm{g}}} = \frac{P_{\mathrm{H_2O}}^{\mathrm{g}}(T)}{P_{\mathrm{T}}} \tag{10}$$

If the mass transfer of water from the liquid phase to the gas phase is not fast enough, the gas phase becomes progressively saturated along the axial reactor coordinate, leading to

$$\frac{1}{A}\frac{\mathrm{d}\dot{n}_{\mathrm{H_2O}}^{\mathrm{g}}}{\mathrm{d}z} + k_{\mathrm{G}}a\left(C_{\mathrm{H_2O}}^{\mathrm{g}} - \frac{P_{\mathrm{H_2O}}^{\mathrm{g}}(T)}{RT}\right) = 0 \tag{11}$$

$$C_{\mathrm{H_2O}}^{\mathrm{g}} = \frac{\dot{n}_{\mathrm{H_2O}}^{\mathrm{g}}}{\dot{n}_{\mathrm{T}}^{\mathrm{g}}}\frac{P_{\mathrm{T}}}{RT} \tag{12}$$

The total system pressure P_{T}, being only marginally affected by the pressure drop throughout the bed under the given operating conditions, is considered to be constant in the model.

Neglecting incomplete cold gas saturation, it follows that

$$\dot{n}_{\mathrm{H_2O}}^{\mathrm{g}} = (\dot{n}_{\mathrm{H_2O}}^{\mathrm{g}})_{\mathrm{inlet}} + \int_0^z \varphi(z)\,\mathrm{d}z \tag{13}$$

$$\dot{n}_{\mathrm{T}}^{\mathrm{g}} = (\dot{n}_{\mathrm{T}}^{\mathrm{g}})_{\mathrm{inlet}} + \int_0^z \varphi(z)\,\mathrm{d}z \tag{14}$$

The fluid temperature and the total molar gas and liquid flow rates undergo changes along the FBR length, and the gas and liquid superficial velocities have to be adjusted accordingly. For the gas phase, the axial variation of the superficial velocity is calculated assuming ideal gas behavior:

$$u_{\mathrm{g}} = \frac{\dot{V}_{\mathrm{g}}}{A} = \frac{\dot{n}_{\mathrm{T}}^{\mathrm{g}} RT}{P_{\mathrm{T}}A} \tag{15}$$

Differentiation leads to

$$\frac{\mathrm{d}u_{\mathrm{g}}}{\mathrm{d}z} = \frac{RT}{P_{\mathrm{T}}A}\varphi + \frac{\dot{n}_{\mathrm{T}}^{\mathrm{g}} R}{P_{\mathrm{T}}A}\frac{\mathrm{d}T}{\mathrm{d}z} \tag{16}$$

For the dynamic liquid phase, the change in the superficial velocity is calculated respectively using the liquid density of pure water:

$$\frac{\mathrm{d}u_{\mathrm{l}}}{\mathrm{d}z} = \frac{\mathrm{d}}{\mathrm{d}z}\left(\frac{\dot{m}_{\mathrm{l}}}{A\rho_{\mathrm{l}}}\right) = \frac{\dot{m}_{\mathrm{l}}}{A}\frac{\mathrm{d}}{\mathrm{d}T}\left(\frac{1}{\rho_{\mathrm{l}}}\right)\frac{\mathrm{d}T}{\mathrm{d}z} + \frac{1}{A\rho_{\mathrm{l}}}\frac{\mathrm{d}\dot{m}_{\mathrm{l}}}{\mathrm{d}z} \tag{17}$$

The boundary conditions for the reactor-scale model are as follows:

At the reactor entrance ($z = 0$):

$$C_{\mathrm{O_2}}^{\mathrm{g}} = (C_{\mathrm{O_2}}^{\mathrm{g}})_{\mathrm{inlet}} \tag{18}$$

$$u_{\mathrm{l}}(C_j^{\mathrm{d}})_{\mathrm{inlet}} = u_{\mathrm{l}} C_j^{\mathrm{d}}|_{z=0^+} - \epsilon_{\mathrm{ld}} D^{\mathrm{ad}}\frac{\partial C_j^{\mathrm{d}}}{\partial z} \tag{19}$$

$$T = T_{\mathrm{inlet}} \tag{20}$$

At the reactor outlet ($z = L_{\mathrm{R}}$):

$$\frac{\partial C_j^{\mathrm{d}}}{\partial z} = 0 \tag{21}$$

Table 2. Values of Physical Properties in the Range of Operating Conditions Used

property	120 °C	140 °C	160 °C	ref
ρ_{H_2O}, kg/m^3	943	926	908	18
μ_{H_2O}, Pa s $\times 10^4$	2.34	1.93	1.75	18
σ_{H_2O}, N/m $\times 10^2$	5.69	5.38	5.08	18
$P^g_{H_2O}$, MPa	0.199	0.362	0.619	18
c_{pl}, kJ/(kg K)	4.24	4.28	4.34	18
c_{pg}, kJ/(kg K)	1.05	1.05	1.05	18
ΔH^v, kJ/mol	40.2	39.13	38	18
ΔH^{com},[a] kJ/mol	−3000	−3000	−3000	18
D_{O_2}, m^2/s $\times 10^{-8}$	1.72	2.35	3.12	19
D_{phenol}, m^2/s $\times 10^{-8}$	0.528	0.671	0.779	18[b]
H, MPa $\times 10^{-3}$	6.83	6.25	5.53	20

[a] Heat of phenol combustion to form CO_2 and H_2O. [b] Wilke−Chang, 1955, in ref 18.

Physical Properties, Hydrodynamic and Mass- and Heat-Transfer Parameters. Pure water and air or gas mixture properties are considered for the bulk liquid and gas phases. Water and gas heat capacities, water heat of evaporation, heat of phenol combustion, water vapor pressure, water density, and phenol diffusion coefficients have been obtained from data or methods included in work by Reid et al.[18] Dissolved oxygen diffusion coefficient and Henry constants for oxygen solubility in water are taken from work by Diaz et al.[19] and Himmelblau,[20] respectively. Table 2 gives values of these parameters calculated for the temperature range studied.

The quality of the prediction of the packed-bed model depends primarily on the accuracy of the involved model parameters. Kinetic parameters have been assessed from suitable experiments.[14] For the other key parameters, the available literature correlations have been examined to select appropriate values. However, this turns out to be a difficult task because there can exist a very large dispersion between the results calculated from the specific correlations. Hydrodynamic and transport parameters strongly depend on the nature of the gas−liquid flow through the bed. For cocurrent two-phase upflow and bubble-flow regimes, the liquid phase is continuous and the packed-bed column operates with high liquid holdups and fully wetted pellets. External mass transfer and axial dispersion are thus gaining in importance. When the packed bed is operated in a trickle downflow regime, the gas phase becomes the continuous phase and partial wetting of the pellets may occur. In this situation, external mass transfer and axial dispersion can be less influent, whereas the pellet wetting efficiency is thought to be crucial for the reactor conversion. Table 3 lists both the literature correlations selected and a set of values of key model parameters.

3.3. Numerical Solution. The PDE model in combination with the classical pore diffusion model is applied to describe the performance of the packed-bed pilot-plant reactor. A sequential approach is performed to numerically solve the corresponding equation system.

The pellet- and reactor-scale models lead to a set of algebraic−differential equations that involve nonlinear reaction rates. To solve these model equations with boundary constraints, the robust numerical method of orthogonal collocation on finite elements has been used.[21] In most situations, eight collocation points have been sufficient to readily obtain model convergence for both reactor and pellet length scales with only one finite element.

4. Results and Discussion

4.1. Phenol Oxidation over AC in Laboratory-Scale FBRs. Catalytic Performance of AC in a TBR. The phenol conversion space-time profiles obtained in downflow operation are given in Figure 2 for oxygen partial pressures and temperatures of 0.1 and 0.2 MPa and 120, 140, and 160 °C, respectively. The phenol destruction is seen to improve strongly with increasing temperature, pressure, and liquid space time. At low conversion of phenol, mineralization of the reacted phenol to CO_2 and H_2O is almost complete, while the difference between the phenol and COD conversions becomes larger as the phenol conversion increases. At 160 °C and 0.2 MPa, phenol and COD destructions beyond 99% and 85%, respectively, are achieved for space times greater than 0.4 h. Compared to recently developed catalysts,[11] the AC studied displays thus a comparable or even better catalytic performance in phenol CWAO at 160 °C but a significantly lower oxygen partial pressure of 0.2 MPa.

The main intermediates detected are 4-hydroxybenzoic acid (because of some interaction with AC, 4-hydroxybenzoic acid usually not being found with other catalysts), benzoquinone, and maleic, formic, and acetic acids as well as traces of hydroquinone, catechol, and oxalic acid. The AC catalyst exhibited accumulation of refractory acetic acid, which accounts for 15% of the liquid-phase COD remaining at the highest phenol conversions.

Comparison of a TBR and a Flooded-Bed Reactor. Gas−liquid hydrodynamic and mass-transfer pa-

Table 3. Parameter Values and Correlations Used in Upflow and Downflow Reactor Modeling of a Pilot Plant at T = 140 °C, P_T = 0.6 MPa, Q_G = 100 NL/h, and F_L = 0.5 kg/h

parameter	downflow operation mode		upflow operation mode	
D^{ad}, m^2/s	2.2×10^{-5}	Michell and Furzer,[33] 1992	6.4×10^{-5}	*a*
$D^{eff}(Ph/O_2)$, m^2/s	$(1.2/4.2) \times 10^{-9}$	*b*	$(1.2/4.2) \times 10^{-9}$	*b*
k_{gs}, m/s	3.8×10^{-2}	Dwivedi and Upadhyay,[34] 1977		
$k^d_{ls}(Ph/O_2)$, m/s	$(1.4/3.1) \times 10^{-4}$	Tan and Smith,[35] 1982	$(3.2/7.3) \times 10^{-4}$	Specchia et al.,[41] 1978
$k^s_{ls}(Ph/O_2)$, m/s	$(0.9/2.1) \times 10^{-6}$	Iliuta et al.,[36] 1999	$(0.9/2.1) \times 10^{-6}$	Iliuta et al.,[36] 1999
$(ka)_{ll}$, s^{-1}	1.0×10^{-2}	Hochmann and Effron,[37] 1969	1.0×10^{-2}	Hochmann and Effron,[37] 1969
k_La, s^{-1}	8.1×10^{-2}	Morsi,[30] 1989	1.3×10^{-1}	Saada,[28] 1972
ϵ_{ld}	0.10	Ellman et al.,[38] 1990	0.22	Yang et al.,[42] 1989
ϵ_{ls}	0.05	Saez and Carbonell,[39] 1985	0.05	Saez and Carbonell,[39] 1985
f[c]	0.68 (or 1)	El-Hisnawi et al.,[40] 1982	1.0	
h_w, W/(m^2 K)	1.1×10^2	*d*	5.1×10^2	Sokolov and Yablokova,[25] 1983

[a] Axial dispersion estimated by Stüber[29] (correlation derived from Syaiful[43]). [b] Calculated assuming tortuosity factor = 3. [c] The static, f_s, and dynamic, f_d, components of the wetting efficiency f were obtained from the approximation of Rajashekharam et al.:[44] $f_s/f_d = \epsilon_{ls}/\epsilon_{ld}$. [d] Estimated to match the experimental axial temperature profiles (the correlation of Mariani et al.[26] is then used to calculate the variation of h_w within the range of operating conditions).

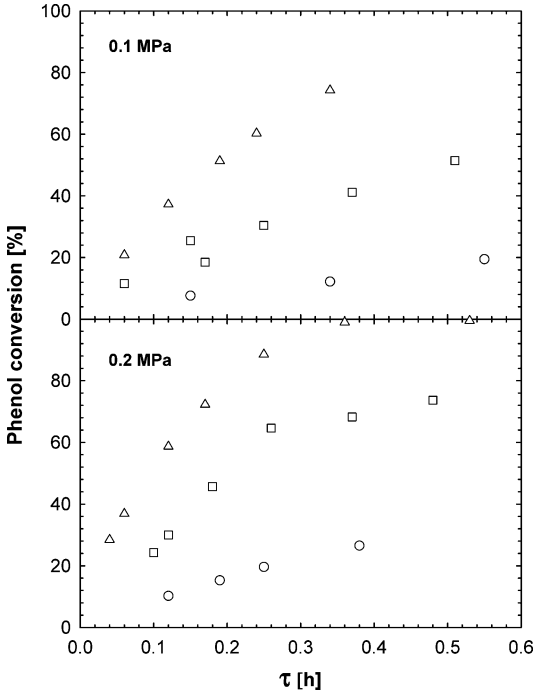

Figure 2. Experimental phenol conversions in the downflow mode at 0.1 and 0.2 MPa and different temperatures: (○) 120 °C; (□) 140 °C; (△) 160 °C.

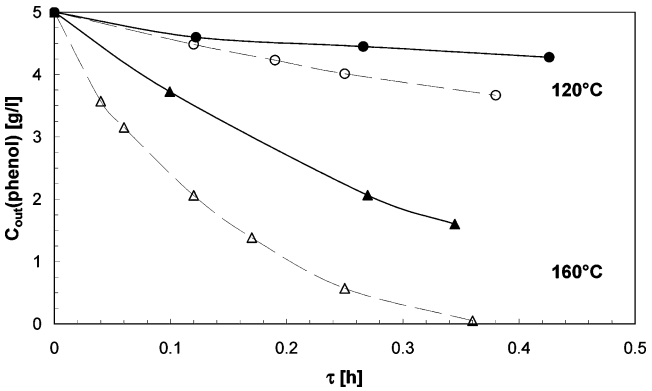

Figure 3. Phenol concentration for downflow (open symbols) and upflow (filled symbols) oxidation over AC at 0.2 MPa of O_2. Lines indicate trends.

rameters are key parameters for the understanding of the performance of FBRs. Here, it is shown with the help of three-phase reactor flow maps that the TBR always operated in the trickle-flow regime. Because of its low solubility, oxygen though in large excess is the limiting reactant, as calculated by Khadilkar et al.[22]

In the trickle-flow regime, the external liquid holdup takes small values of around 0.1 and the catalyst wetting efficiency is estimated to range between 0.25 and 0.5 at the liquid flow rates used.[23,24] Because the gas−solid mass transfer is generally 1 or 2 orders of magnitude higher (see Table 3) than that at the liquid−solid interface, the liquid-filled pores that connect to the "dry" particle surface are always saturated with oxygen. Partial wetting in the downflow mode should then positively affect the catalyst performance. This trend is clearly confirmed in Figure 3, which compares the reactor performance for both a fully wetted upflow mode and a partially wetted downflow mode. The downflow mode occurring in the kinetically controlled regime yields substantially lower phenol outlet concentrations

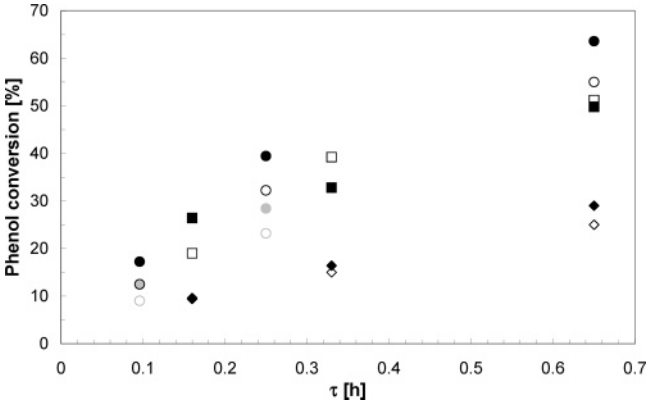

Figure 4. Phenol conversion as a function of the liquid space time for downflow (open symbols) and upflow (filled symbols) at different oxygen partial pressures: (◇) 0.05 MPa; (□) 0.12 MPa; (○) 0.2 MPa. $u_{g,inlet} = (1.1-1.2) \times 10^{-2}$ m/s; $T_w = 140$ °C. Gray symbols show experimental results without correction by catalyst deactivation.

(i.e., higher phenol conversions) in all conditions tested. The fully wetted upflow mode is therefore limited by the presence of gas−liquid mass-transfer limitations of oxygen and probably some degree of axial dispersion at the lowest liquid flow rates.

4.2. Scale-up of Phenol Oxidation over AC. The phenol oxidation has also been performed in a jacketed pilot-plant reactor to scale up the process and assess its performance under eventually mass-transfer-limited and nonisothermal conditions.

The experimental standard procedure, as described in section 2.2, includes steps of reactor start-up, steady state of the reaction, and regular control of the catalyst activity. Steady-state conditions of the reaction are verified through transient sampling. Transient periods to reach steady state (from 1.5 to 4 h) mainly depend on the liquid flow rate selected as well as the operating conditions of the previous run, leading to different preliminary adsorption times. The catalyst activity has been regularly checked at the standard conditions of T_{oil} = 140 °C, F_L = 1 kg/h, Q_G = 100 NL/h, and P_{O_2} = 0.12 MPa. No deactivation is observed at 120 and 140 °C after more than 300 h of operation corresponding to 5 g of phenol treated/g of AC. However, at the highest reaction temperature of 160 °C, the catalyst activity is quickly reduced by 20% after a few runs of 30 h in total.

In the experimental series, the four main operating parameters (T_{oil}, P_{O_2}, u_l, and u_g) and flow direction have been investigated over a wide range of operating conditions (see Table 1). In this way, a large set of steady-state data have been obtained in the pilot-plant reactor. The obtained phenol conversions are displayed as a function of the liquid space time in Figures 4−6 for different pressures, temperatures, and gas velocities, respectively.

The most striking observation is that, contrary to the small-scale FBR experiments, both upflow and downflow modes lead to very similar phenol conversions at any condition. This result is confirmed by the standard deviation between upflow and downflow that is calculated to about 12% without any correlation to the four operating parameters studied. Another important difference is found for the distribution of reaction intermediates. Phenol oxidation in the pilot-plant FBR results in much less maleic acid but much more malonic and oxalic acids. Also, the formic acid concentration is double, whereas the acetic acid concentration is 4 times

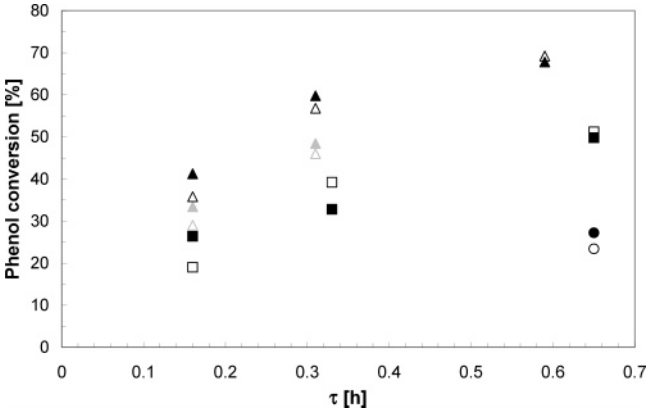

Figure 5. Phenol conversion as a function of the liquid space time for downflow (open symbols) and upflow (filled symbols) at different wall temperatures: (○) 120 °C; (□) 140 °C; (△) 160 °C. $u_{g,inlet} = (1.1-1.2) \times 10^{-2}$ m/s; $P_{O_2} = 0.12$ MPa. Gray symbols show experimental results without correction by catalyst deactivation.

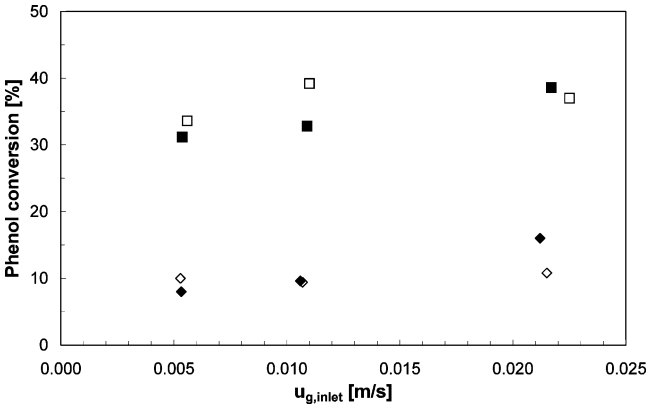

Figure 6. Phenol conversion as a function of the gas velocity for downflow (open symbols) and upflow (filled symbols) at different operating conditions ($T_w = 140$ °C): (◇) $P_{O_2} = 0.05$ MPa and $F_L = 2$ kg/h; (□) $P_{O_2} = 0.12$ MPa and $F_L = 1$ kg/h.

less. Only the concentrations of aromatic compounds remain similarly low in the two FBRs.

As expected from the batch kinetic study, phenol conversion significantly increases with the partial oxygen pressure (Figure 4) and temperature (Figure 5) in rough agreement with kinetics. On the other hand, the gas velocity has only a very small effect (Figure 6) in both operation modes. If in the downflow mode external mass-transfer coefficients are known to depend mostly on the liquid velocity, a more marked positive effect would be expected in the upflow mode. Actually, the poor effect of the gas flow rate could be explained either by the marginal effect of external mass transfer in quasi-kinetic control or by its balanced influences on mass transfer and on vaporization. This situation of different external mass transfer and its effect on the FBR performance will be detailed in section 4.3.

On the whole, it can be concluded that the scale-up of phenol CWAO over AC based on a simple liquid space-time analogy would lead to an erroneous reactor design, which clearly highlights the need for the development of detailed reactor models to predict the reactor performance on different reactor scales.

4.3. Prediction of the Pilot-Plant Reactor Performance. The pilot-plant reactor data have been thoroughly analyzed with the detailed PDE model developed in section 3.2. In addition to physicochemical properties and thermodynamic and kinetic data, the

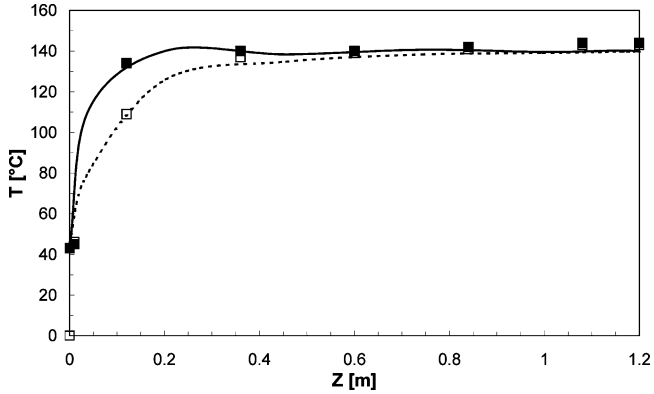

Figure 7. Axial temperature profiles for $P_{O_2} = 0.12$ MPa, $T_w = 140$ °C, $u_{g,inlet} = 1.1 \times 10^{-2}$ m/s ($Q_G = 100$ NL/h), and $F_L = 1$ kg/h. Symbols show experimental results. Lines show simulation: upflow mode (filled symbols, solid line); downflow mode (open symbols, short dotted line).

packed-bed reactor model requires the input of several key parameters such as the wall-to-bed heat-transfer coefficient, the liquid- and gas-side volumetric mass-transfer coefficients, both for oxygen absorption and water vaporization, and the liquid−solid mass-transfer coefficient. For trickle-bed simulation, the situation is even more complex, including partial catalyst wetting. The accurate prediction of all of these parameters is a critical task for successful reactor modeling. Various correlations exist for the main model parameters, although a dramatic spreading of up to 2 orders of magnitude can result from their application, as in the case of the volumetric gas−liquid mass-transfer coefficient. A large difference is also found for the liquid axial dispersion coefficient in upflow operation. Moreover, for the most refined trickle-bed model, some model parameters cannot even be estimated because of the lack of specific correlations.

In the case of phenol CWAO, heat-transfer and axial temperature profiles may be analyzed separately because of relatively high heat transfer (small tube diameter), very low heat production by reaction (diluted phenol), and moderate heat consumption for water vaporization. As shown in Figure 7, the predicted temperatures fit well with the experimental temperature profiles when using the correlation of Sokolov and Yablokova[25] in the upflow mode and a modified correlation of Mariani et al.[26] in the downflow mode (divided by 2). It clearly appears that upflow provides superior wall-to-bed heat-transfer conditions (steeper temperature profiles); nevertheless, even in downflow the reactor temperature reaches the wall temperature after about 30 cm of the catalytic fixed bed. Thus, as a first approximation, the reactor can be considered to operate quasi-isothermally.

The situation of gas−liquid upflow operation being less complex will be examined first. The sensibility of the reactor performance to oxygen mass transfer and water vaporization is not straightforward. In the nonisothermal reactor zone (first 30 cm of the fixed bed), the water vapor pressure increases exponentially and the induced water vaporization reduces gradually the oxygen partial pressure in the gas phase and at the same time increases the phenol concentration in the remaining liquid and the liquid space time. The effect of vaporization is rarely accounted for in modeling and, therefore, two vaporization rates have been implemented and compared: either instantaneous vapor−

Table 4. Influence of k_La, k_Ga, and D^{ad} on the Upflow Model Conversion: Comparison with the Reference Case and Experimental Conversion at T_{oil} = 140 °C, F_L = 0.5 kg/h, Q_G = 100 NL/h, and P_{O_2} = 0.12 MPa

k_La/k_La(Saada)	k_Ga/k_La	D^{ad}/D^{ad}(Stüber)	ΔX_{rel} (%)[a]	ΔX_{rel} (%)[b]
1	∞	1	0	−5.5
1	5	1	7.7	1.8
1	1	1	26.7	19.7
0.2	∞	1	−84.3	−85.2
0.2	5	1	−56.2	−58.7
0.2	1	1	−15.5	−20.1
5	∞	1	30.1	23
5	5	1	31.4	24.2
5	1	1	35.3	27.8
1	∞	4.2	−4	−9.3
5	1	4.2	26.9	19.8

[a] Relative difference with respect to conversion obtained from the simulated reference case of line 1. [b] Relative difference with respect to experimental conversion.

liquid equilibrium, i.e., infinitely fast vaporization, or mass-transfer-limited vaporization, involving the gas-side volumetric mass-transfer coefficient (k_Ga). This parameter is not well-known for either upflow or for downflow, where it has been reported to be at least equal to the liquid-side mass-transfer coefficient.[27]

To assess the influence of water vaporization on the upflow reactor performance, a set of simulations with $k_Ga = k_La$, $k_Ga = 5k_La$, and $k_Ga = \infty$ (equilibrium) have been carried out. The Saada[28] correlation is used to calculate k_La, and in the following, the obtained k_La values are multiplied and divided by 5. The results of the sensitivity study are summarized in Table 4 for the reference conditions of T_{oil} = 140 °C, Q_G = 100 NL/h, and P_{O_2} = 0.12 MPa. A lower liquid flow rate of F_L = 0.5 kg/h has been selected both to achieve a larger phenol conversion and to test the effect of axial dispersion in the liquid phase.

For the axial dispersion coefficients studied, only a limited change of outlet phenol conversion (always less than 7%) has been observed in the simulation runs. Thus, it can be concluded that axial dispersion effects do not play a significant role for phenol conversion under the given operating conditions. Simulation results are first compared with the reference case (k_La from Saada[28] and instantaneous equilibrium and axial dispersion from Stüber[29]) and then with the experimental conversion (last column of Table 4). With respect to the gas−liquid mass transfer, at high k_La values (5 times higher), the vaporization rate (k_Ga) has nearly no influence on conversion increasing slowly from 30.1 to 35.3%, although the experimental conversion is overestimated by 23−27.8%. The situation becomes very different at low k_La values (5 times smaller) that can generate a very large underestimation of the conversion up to −85% depending on the vaporization rate (k_Ga). This suggests that the gas−liquid mass transfer in upflow operation is only moderately limiting the reactor conversion. The Saada[28] correlation giving the best agreement with the experimental data will be further used in the model predictions.

Parts a and b of Figure 8 show profiles of the experimental exit phenol concentration and corresponding simulations for upflow operation. It is seen that the best agreement with the experimental data is found for a relation of k_G/k_L = 5. Nevertheless, in the range of conditions studied in this work, it appears that the rate of water evaporation does not significantly change the outlet concentration and vapor−liquid equilibrium could be assumed for simplicity.

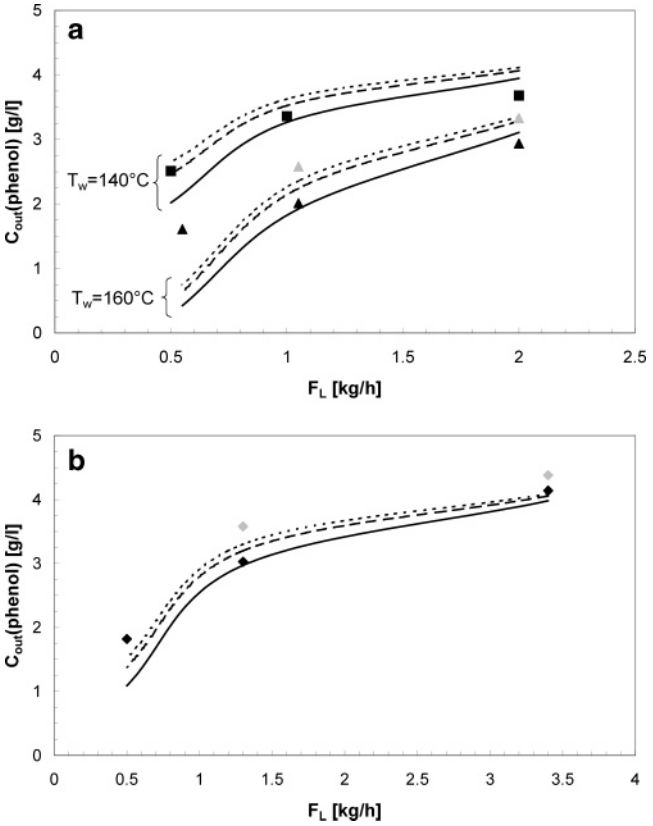

Figure 8. Upflow outlet phenol concentrations: experimental results (symbols) and corresponding simulations for a fully wetted catalyst: $k_Ga = k_La$ (solid line); $k_Ga = 5k_La$ (long dotted line); instantaneous liquid−vapor equilibrium (short dotted line). (a) P_{O_2} = 0.12 MPa: (■) T_w = 140 °C. Q_G = 100 NL/h*; (▲) T_w = 160 °C. Q_G = 175 NL/h*. (b) P_{O_2} = 0.2 MPa: (◆) T_w = 140 °C. Q_G = 100 NL/h*. Asterisks indicate the same inlet gas velocity: $u_{g,inlet}$ = 1.1×10^{-2} m/s. Gray symbols show experimental results without correction by catalyst deactivation.

Table 5. Influence of the Particle Wetting Efficiency on the Simulated Outlet Phenol Concentration in the Downflow Mode: P_{O_2} = 0.12 MPa, T_w = 140 °C, Q_G = 100 NL/h, F_L = 0.5 kg/h, case k_Ga = ∞

f	1	0.9999	0.9	0.68[a]
$C_{Ph,out}$, g/L	3.22	2.18	2.02	2.02

[a] Calculated from the El-Hisnawi[40] correlation.

However, the slightly positive effect of increasing gas velocity on the phenol conversion observed experimentally in the upflow mode could not be checked by the model. If k_Ga is equal to k_La, model predictions show nearly no influence on the gas velocity, or an increase of the phenol outlet concentration due to higher water vaporization flux for higher values of k_Ga.

The simulation of the TBR is even more complex when involving partial catalyst wetting, which is found to have a strong impact on the reactor performance as shown in Table 5. As soon as full wetting is not assumed (f < 1), mass transfer to the dry zone becomes extremely fast and oxygen mass-transfer limitation vanishes. This large overestimation of the effect of catalyst wetting in the model is due to the assumption of a uniform concentration at the catalyst surface whether wet or dry. As a consequence, there is no sensitivity to the value of the external wetting efficiency, with the only important hypothesis being either fully or partially wetted conditions. Indeed, there is no simple way to account for multidirectional pore diffusion resulting from nonuni-

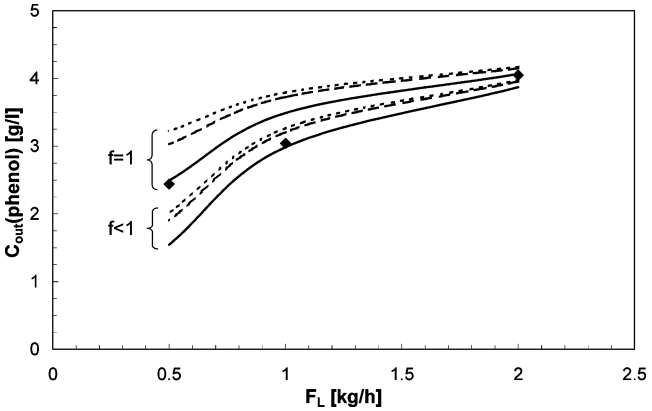

Figure 9. Downflow outlet phenol concentrations: experimental results (◆) and corresponding simulations for fully ($f = 1$) and partially ($f < 1$) wetted catalysts: $k_Ga = k_La$ (solid line); $k_Ga = 5k_La$ (long dotted line); instantaneous liquid−vapor equilibrium (short dotted line). $P_{O_2} = 0.12$ MPa: $T_w = 140$ °C. $Q_G = 100$ NL/h.

form oxygen transfer to the catalyst surface. The use of a different overall effectiveness factor for each zone could be a solution, but it would be very difficult to implement when limitations due to both the liquid and dissolved gaseous reactant are present.

The volumetric mass-transfer coefficient remains then one key model parameter. The correlation of Morsi[30] gives a lower value than that for the upflow mode in similar operating conditions.[31,32] In Figure 9, experimental downflow data are thus compared to those of the two models of either full or partial catalyst wetting. In general, the experimental data lie mostly between the two simulations, with oxygen mass transfer being too fast with any partial wetting and too slow at full wetting.

These simulation results indicate that the opposite roles of oxygen mass transfer and water vaporization are not simply balanced and may have different importance depending on the reaction and hydrodynamic conditions. This situation is not often addressed in modeling of a FBR involving oxidation in the liquid phase, though corresponding to typical industrial conditions for CWAO, and thus should deserve further research work.

5. Conclusions

The performances of laboratory-scale and pilot-plant FBRs have been assessed for CWAO of phenol over AC at mild conditions. The laboratory-scale FBR performs high phenol and COD destructions of 99% and 85% in the downflow mode at 160 °C, 0.2 MPa of oxygen partial pressure, and a space time of 0.4 h. The upflow mode, however, leads to lower phenol outlet conversions because of fully wetted catalyst pellets and stronger gas−liquid mass-transfer limitations. In contrast, in the pilot-plant reactor, similar outlet phenol concentrations have been obtained for both gas−liquid flow directions over the whole range of operating conditions studied. Moreover, the distribution of partial oxidation products is found to depend on the reactor size. In view of the distinct reactor performance, it is clear that the scale-up of the FBR for phenol CWAO based on a mere space-time analogy cannot be recommended.

The pilot-plant reactor has been simulated by a complex nonisothermal, one-dimensional PDE model, which includes different vaporization rates during nonisothermal operation. The effect of water vaporization on the reactor performance is shown to be important, although it is rarely included in the modeling of CWAO reactors. On the whole, the model predictions match conveniently the experimental pilot-plant data for both flow directions. The model developed represents with adequate precision the complex interplay of reaction kinetics, hydrodynamics, and mass-transfer phenomena assuming the absence of radial temperature and concentration gradients. It is thus a very useful tool to support the proper design of industrial CWAO units and can avoid the drawbacks of the too simple space-time approach.

Acknowledgment

We are indebted to the Departament d'Universitats, Recerca i Societat de la Informació de la Generalit de Catalunya, for providing financial support to F.S. (ABM/acs/AIRE-CTP2003-3), and the Thailand Research Fund for providing financial support to S.S. through the Royal Golden Jubilee Ph.D. Program (Grant PhD/0180/2544).

Nomenclature

A = reactor section area (m^2)
C_j = concentration of compound j (mol/m^3)
$C^g_{H_2O}$ = gas-phase concentration of water vapor (mol/m^3)
c_{pl} = liquid heat capacity [J/(kg K)]
c_{pg} = gas heat capacity [J/(kg K)]
D_j = diffusion coefficient of compound j (m^2/s)
D^{eff}_j = effective diffusion coefficient of compound j (m^2/s)
D^{ad} = axial dispersion coefficient (m^2/s)
E = activation energy (J/mol)
f = external wetting efficiency ($f = f_d + f_s$)
F_L = liquid feed flow rate (kg/h)
H = Henry's constant (MPa)
ΔH^v = water enthalpy of vaporization (J/mol)
ΔH_i = heat of the ith reaction (J/mol)
k_0 = preexponential factor of the rate constant of eq 1 [m^3/(s kg)]
k_{gs} = gas−solid mass-transfer coefficient of oxygen (m/s)
k_Ga = gas-side-liquid volumetric mass-transfer coefficient of the water vapor (s^{-1})
k_La = gas−liquid-side volumetric oxygen mass-transfer coefficient (s^{-1})
$(ka)j_{ll}$ = dynamic−static liquid volumetric mass-transfer coefficient of compound j (s^{-1})
k_{jls} = j compound liquid−solid mass-transfer coefficient (m/s)
$\dot{m}_l$ = mass liquid flow rate (kg/s)
$\dot{n}^g_T$ = total molar gas flow rate (mol/s)
$\dot{n}^g_{H_2O}$ = molar water vapor flow rate (mol/s)
$P^g_{H_2O}$ = water vapor pressure (Pa)
P_T = total pressure in the reactor (Pa)
Q_G = gas feed flow rate at normal conditions of T and P (NL/h)
r = particle radial dimension (m)
r_i = ith reaction rate [mol/(kg s)]
r_p = catalyst particle radius (m)
R = universal gas constant [8.314 J/(kg K)]
R_j = total production rate of compound j [mol/(kg s)]
T = temperature (K)
T_w = reactor wall temperature (K)
h_w = wall-to-bed heat-transfer coefficient [W/(m^2 K)]
u_l = liquid superficial velocity (m/s)
u_g = gas superficial velocity (m/s)
V = volumetric flow rate (m^3/s)

V_R = reactor volume (m^3)
W_{cat} = catalyst weight (kg)
x = liquid molar fraction
z = reactor axial dimension (m)

Greek Letters

α = order of reaction of oxygen
ϵ_l = liquid holdup
ϕ' = Weisz modulus for pore diffusion based on the observed reaction rate
η_j = effectiveness factor of compound j
φ = evaporation rate based on the reactor length [mol/(m s)]
μ = viscosity (Pa s)
ρ_b = apparent bed density (kg/m^3)
ρ_l = liquid density (kg/m^3)
ρ_g = gas density (kg/m^3)
ρ_p = catalyst particle density (kg/m^3)
σ = surface tension (N/m)
τ = space time, defined as $\tau = W_{cat}/F_L$ (h)

Superscripts

ap = apparent
d = dynamic liquid
g = gas or dry zone
s = static liquid
* = on the catalyst surface

Subscripts

0 = at the entrance of the reactor
b = bed
d = dynamic liquid
H_2O = water
i = reaction index
j = compound index
O_2 = oxygen
p = particle
Ph = phenol
s = static liquid
T = total
w = wall

Note Added after ASAP Publication. This article was released ASAP on June 8, 2005, with an error in the description of the diffusion model following eq 4. The version posted on June 15, 2005, and the printed version are correct.

Literature Cited

(1) Matatov-Meytal, Y. I.; Sheintuch, M. Catalytic abatement of water pollutants. *Ind. Eng. Chem. Res.* **1987**, *37*, 309.

(2) Pintar, A.; Besson, M.; Gallezot, P. Catalytic wet air oxidation of Kraft bleach plant effluents in a trickle bed reactor over a Ru/TiO_2 catalyst. *Appl. Catal. B* **2001**, *31*, 275.

(3) Hussain, S. T.; Sayari, A.; Larachi, F. Enhancing the stability of Mn−Ce−O WETOX catalysts using potassium. *Appl. Catal. B* **2001**, *34*, 1.

(4) Suarez-Ojeda, M. E.; Stüber, F.; Fortuny, A.; Fabregat, A.; Carrera, J.; Font, J. Catalytic wet air oxidation of substituted phenols using active carbon catalyst. *Appl. Catal. B* **2005**, *19*, 165.

(5) Polaert, I.; Wilhelm, A. M.; Delmas, H. Phenol wastewater treatment by a two-step adsorption−oxidation process on activated carbon. *Chem. Eng. Sci*. **2002**, *57*, 1585.

(6) Mantzavinos, D.; Sahibzada, M.; Livingston, A. G.; Metcalfe, I. S.; Hellgardt, K. Wastewater treatment: wet air oxidation as a precursor to biological treatment. *Catal. Today* **1999**, *53*, 93.

(7) Pintar, A.; Levec, J. Catalytic liquid-phase oxidation of phenol aqueous solutions. A kinetic investigation. *Ind. Eng. Chem. Res*. **1994**, *33*, 3070.

(8) Tukac, V.; Vokál, J.; Hanika, J. Mass transfer limited wet oxidation of phenol. *J. Chem. Technol. Biotechnol*. **2001**, *76*, 506.

(9) Stüber, F.; Polaert, I.; Delmas, H.; Font, J.; Fortuny, A. Fabregat, A. Catalytic wet air oxidation of phenol using active carbon: performance of discontinuous and continuous reactors. *J. Chem. Technol. Biotechnol.* **2001**, *76*, 743.

(10) Grant, T. M.; Judson King, C. Mechanism of irreversible adsorption of phenolic compounds by activated carbons. *Ind. Eng. Chem. Res.* **1990**, *29*, 264.

(11) Stüber, F.; Font, J.; Fortuny, A.; Bengoa, C.; Eftaxias, A.; Fabregat, A. Carbon materials and catalytic wet air oxidation of organic pollutants in wastewater. *Top. Catal*. **2005**, in press.

(12) Maugans, C. B.; Akgerman, A. Catalytic wet oxidation of phenol in a trickle bed reactor over a Pt/TiO_2 catalyst. *Water Res.* **2003**, *37*, 319.

(13) Eftaxias, A.; Larachi, F.; Stüber, F. Modelling of trickle bed reactors for the catalytic wet air oxidation of phenol. *Can. J. Chem. Eng*. **2003**, 784.

(14) Suwanprasop, S. Aromatisation of *n*-hexane and natural gasoline over ZMS-5 zeolite and wet catalytic oxidation of phenol on fixed bed of active carbon. Ph.D. Thesis, Chulalongkorn University (Bangkok, Thailand) and INP Toulouse (France), 2005.

(15) Eftaxias, A. Catalytic Wet Air Oxidation of Phenol in a Trickle Bed Reactor: Kinetics and Reactor Modelling. Ph.D. Thesis, Universitat Rovira i Virgili, Tarragona, Spain, 2003.

(16) Julcour, C.; Le Lann, J. M.; Wilhelm, A. M.; Delmas, H. Dynamics of internal diffusion during the hydrogenation of 1,5,9-cyclododecatriene on Pd/Al_2O_3. *Catal. Today* **1999**, *48*, 147.

(17) Van Gelder, K. B.; Borman, P. C.; Weenink, R. E.; Westerterp, K. R. Three-phase packed bed reactor with an evaporating solvent—II. Modelling of the reactor. *Chem. Eng. Sci*. **1990**, *45* (10), 3171.

(18) Reid, R. C.; Prausnitz, J. M.; Pauling, B. E. *The properties of gases and liquids*; McGraw-Hill: New York, 1987.

(19) Diaz, M.; Vega, A.; Coca, J. Correlation for the estimation of gas−liquid diffusivity. *Chem. Eng. Commun.* **1987**, *52*, 271.

(20) Himmelblau, D. M. Solubilities of inert gases in water: 0 °C to near the critical point of water. *J. Chem. Eng. Data* **1960**, *5*, 10.

(21) Finlayson, B. A. *Nonlinear analysis in chemical engineering*; McGraw-Hill: New York, 1980; p 113.

(22) Khadilkar, M. R.; Wu, Y.; Al-Dahhan, M. H.; Dudukovic, M. P.; Colakyan, M. Comparison of trickle-bed and upflow reactor performance at high pressure: model predictions and experimental observations. *Chem. Eng. Sci.* **1996**, *51*, 2139.

(23) Iliuta, I.; Larachi, F.; Grandjean, B. P. A. Catalyst wetting in trickle flow reactors: a phenomenlogical model. *Chem. Eng. Res. Des.* **1999**, *77*, 759.

(24) Al-Dahhan, M. H.; Dudukovic, M. P. Catalyst wetting efficiency in trickle-bed reactors at high pressure. *Chem. Eng. Sci.* **1995**, *50*, 2377.

(25) Sokolov, V. N.; Yablokova, M. A. Thermal conductivity of a stationary granular bed with upward gas−liquid flow. *J. Appl. Chem. USSR* **1983**, *56*, 551.

(26) Mariani, N. J.; Martinez, O. M.; Barreto, G. F. Evaluation of heat transfer parameters in packed beds with cocurrent downflow of liquid and gas. *Chem. Eng. Sci.* **2001**, *56*, 5995.

(27) Gianetto, A.; Silveston, P. L. *Multiphase Chemical Reactors: Theory, Design, Scale-Up*; Hemisphere Publishing: Bristol, PA, 1986.

(28) Saada, M. Y. Assessment of interfacial area in co-current two-phase flow in packed beds. *Chim. Ind., Génie Chim.* **1972**, *105* (20), 1415.

(29) Stüber, F. Sélectivité en réacteur catalytique triphasique: analyse expérimentale et théorique d'hydrogénations consécutives en lit fixe catalytique à co-courant ascendant de gaz et de liquide. Ph.D. Thesis, INP, Toulouse, France, 1995.

(30) Morsi, B. I. Mass transfer coefficients in a trickle-bed reactor with high and low viscosity organic solutions. *Chem. Eng. J.* **1989**, *41*, 41.

(31) Goto, S.; Levec, J.; Smith, J. M. Mass transfer in packed beds with two-phase flow. *Ind. Eng. Chem. Process Des. Dev.* **1975**, *14* (4), 473.

(32) Specchia, V.; Sicardi, S.; Gianetto, A. Absorption in packed towers with concurrent upward flow. *AIChE J.* **1974**, *20* (4), 646.

(33) Michell, R. W.; Furzer, I. A. Mixing in trickle flow through packed beds. *Chem. Eng. J.* **1972**, *4*, 53.

(34) Dwivedi, P. N.; Upadhyay, S. N. Particle-fluid mass transfer in fixed and fluidized beds. *Ind. Eng. Chem. Process Des. Dev.* **1977**, *16* (2), 157.

(35) Tan, C. S.; Smith, J. M. A dynamic method for liquid-particle mass transfer in trickle beds. *AIChE J*. **1982**, *28* (2), 190.

(36) Iliuta, I.; Larachi, F.; Grandjean, B. P. A. Residence time, mass transfer and back-mixing of the liquid in trickle flow reactors containing porous particles. *Chem. Eng. Sci.* **1999**, *54* (18), 4099.

(37) Hochman, J. M.; Effron, E. Two-phase cocurrent downflow in packed beds. *Ind. Eng. Chem. Fundam.* **1969**, *8* (1), 63.

(38) Ellman, M. J.; Midoux, N.; Wild, G.; Laurent, A.; Charpentier, J. C. A new improved liquid hold-up correlation for trickle-bed reactors. *Chem. Eng. Sci.* **1990**, *45* (7), 1677.

(39) Saez, A. E.; Carbonell, R. G. Hydrodynamic parameters for gas−liquid cocurrent flow in packed beds. *AIChE J.* **1985**, *31* (1), 52.

(40) El-Hisnawi, A. A.; Dudukovic, M. P.; Mills, P. L. Trickle-bed reactors: dynamic tracer tests, reaction studies, and modeling of reactor performance. *ACS Symp. Ser*. **1982**, *196*, 421.

(41) Specchia, V.; Baldi, G.; Gianetto, A. Solid−liquid mass transfer in concurrent two-phase flow through packed beds. *Ind. Eng. Chem. Process Des. Dev.* **1978**, *17* (*3*), 362.

(42) Yang, X. L.; Euzen, J. P.; Wild, G. Etude de la rétention liquide dans les réacteurs à lit fixe avec écoulement ascendant de gaz et de liquide. *Entropie* **1989**, *150*, 17.

(43) Syaiful. Réacteurs polyphasiques à co-courant ascendant: influence de la viscosité sur les rétentions, dispersions axiales et transfert gaz−liquide. Ph.D. Thesis, INP, Toulouse, France, 1992.

(44) Rajashekharam, R.; Jaganathan, R.; Chaudhari, V. A Trickle Bed Reactor Model for Hydrogenation of 2,4-Dinitrotoluene: Experimental Verification. *Chem. Eng. Sci.* **1998**, *53* (4), 787.

Received for review February 24, 2005
Revised manuscript received April 13, 2005
Accepted May 2, 2005